An extended and revised Lake Suigetsu varve chronology from ~50 to ~10 ka BP based on detailed sediment micro-facies analyses

Schlolaut, Gordon; Staff, Richard A.; Brauer, Achim; Lamb, Henry; Marshall, Michael H.; Ramsey, Christopher Bronk; Nakagawa, Takeshi

Published in:
Quaternary Science Reviews

DOI:
10.1016/j.quascirev.2018.09.021

Publication date:
2018

Citation for published version (APA):
Schlolaut, G., Staff, R. A., Brauer, A., Lamb, H., Marshall, M. H., Ramsey, C. B., & Nakagawa, T. (2018). An extended and revised Lake Suigetsu varve chronology from ~50 to ~10 ka BP based on detailed sediment micro-facies analyses. *Quaternary Science Reviews*, *200*, 351-366. https://doi.org/10.1016/j.quascirev.2018.09.021

An extended and revised Lake Suigetsu varve chronology from ~50 to ~10 ka BP based on detailed sediment micro-facies analyses

Gordon Schlolaut[1,2,*], Richard A. Staff[3,4], Achim Brauer[2], Henry F. Lamb[5], Michael H. Marshall[5], Christopher Bronk Ramsey[4] and Takeshi Nakagawa[6]

(1) Centre for Ocean Drilling Science (ODS), Japan Agency for Marine-Earth Science and Technology (JAMSTEC), 3173-25 Showa-machi, Kanazawa-ku, Yokohama, 236-0001 Japan

(2) Section 5.2: Climate Dynamics and Landscape Evolution, GFZ German Research Centre for Geosciences, Telegrafenberg, 14473 Potsdam, Germany

(3) SUERC, University of Glasgow, Scottish Enterprise Technology Park, Rankine Avenue, East Kilbride, Scotland G75 0QF, UK

(4) Research Laboratory for Archaeology and the History of Art (RLAHA), University of Oxford, Oxford, OX1 3QY, UK

(5) Department of Geography and Earth Sciences, Aberystwyth University, Aberystwyth SY23 3DB, UK

(6) Research Centre for Palaeoclimatology, Ritsumeikan University, 1-1-1 Noji-Higashi Kusatsu, Shiga 525-8577, Japan

*corresponding author; e-mail: SchlolautG@gmail.com

Abstract:

Lake Suigetsu is a key site for radiocarbon (^{14}C) calibration and palaeo-environmental reconstruction in East Asia. Here we present a description of the sediment (micro)facies, which in combination with a new approach to varve interpolation allows construction of a revised varve based chronology that extends the previous 2012 varve based chronology by ~10 ka, back to ~50 ka BP. Challenges in varve counting and interpolation, which were

previously discussed in detail only for the Last Glacial-Interglacial Transition, are described here back to ~50 ka BP. Furthermore, the relative merits of varve counting by µXRF scanning and by thin-section microscopy are discussed. Facies analysis reveals four facies zones, their transitions driven by both local and climatic controls. The lamination quality of the sediment is highly variable and varve interpolation reveals that in the analysed time interval, on average, only 50% of the annual cycles are represented by seasonal layers. In the remaining years seasonal layers are indistinguishable, i.e. either did not form or were not preserved. For varve interpolation an advanced version of the Varve Interpolation Program was used, which enabled the construction of the longest, purely varve dated chronology published, despite long intervals of poor lamination quality. The calculated interpolation uncertainty is +8.9% and -4.6%, which is well within expectations considering the high degree of interpolation and the length of the record.

keywords: palaeolimnology; Lake Suigetsu; Eastern Asia; sedimentology; varve; microfacies; µXRF; varve interpolation

1. Introduction

Lake Suigetsu, located at the west coast of central Japan (Fig. 1), is a unique palaeoenvironmental archive in East Asia. The sediment sequence spans at least the last 150 ka (Nakagawa et al., 2012) and contains annual and seasonal laminae, mostly in the time interval from ~10 to ~50 ka BP. Kitagawa & van der Plicht (1998, 2000) first showed that the archive had the potential to contribute to the international atmospheric radiocarbon calibration dataset (IntCal) using varve counting to derive an independent calendar chronology and terrestrial leaf fossils for ^{14}C dating unaffected by reservoir effects. Furthermore, much work has been carried out on palaeoenvironmental reconstruction based on proxies from the sediment (e.g. Nakagawa et al., 2002, 2003, 2005, 2006, Katsuta et al., 2006, 2007, Tyler et al., 2010, Kossler et al. 2011, Schlolaut et al., 2014, 2017).

While the first major Suigetsu drilling project (‘SG93’) (Kitagawa et al., 1995) suffered from some core quality issues such as incomplete core retrieval (Staff et al., 2010), the successor project (‘SG06’) (Nakagawa et al., 2012) successfully produced a terrestrial radiocarbon calibration dataset (Bronk Ramsey et al., 2012) on a set of continuously overlapping cores over the complete sediment sequence. It is the only terrestrial calibration dataset unaffected by any reservoir or dead carbon effects included in the IntCal13 dataset beyond 13.9 ka BP (Reimer et al., 2013). In addition, Lake Suigetsu is highly suitable for tephrochronology (Smith et al., 2013, McLean et al., 2016). For all these reasons Lake Suigetsu is a key site with respect to geochronology, palaeoecology and palaeoclimatology.

Here we describe the most significant facies and microfacies changes in the time interval ~10 to ~50 ka BP alongside a revised and extended varve based chronology for this time interval. Understanding facies and microfacies changes is essential for the creation of the chronology, understanding its uncertainties as well as for further proxy analysis, since microfacies data can help to distinguish climatic and local controls on different proxies. While Suigetsu varve chronologies beyond the Last Glacial-Interglacial Transition (LGIT) have been used in previous publications (e.g. Kitagawa & van der Plicht 1998, 2000, Bronk Ramsey et al., 2012), only the sediments and varve characteristics of the LGIT have been previously described in detail (Schlolaut et al., 2012).

To improve the Suigetsu varve based chronology compared to the 2012 varve based chronology (Bronk Ramsey et al., 2012) we use an advanced version of the Varve Interpolation Program (VIP version 3.0.0) (Schlolaut, 2018). Since the Suigetsu varve count requires a relatively high interpolation rate of about 50%, we refer to the chronology as ‘varve based’ rather than just as ‘varve’ chronology. We also revise our previous approach for combining count datasets from different counting methods and different quality selective datasets (Marshall et al., 2012). Furthermore, the varve count data are extended by approximately 10,000 years to ~50 ka BP. In sediments older than ~50 ka BP seasonal layers occur only very infrequently and are insufficient for a reliable further extension of the varve chronology.

1.1 Study site

Lake Suigetsu is situated in Fukui prefecture on the west coast of Honshu Island, central Japan (35°35’N, 135°53’E, 0 m above sea level). It is part of a tectonic lake system (Mikata Five Lakes) with the active Mikata fault running N-S less than 2 km to the east (Fig. 1). The lake is approximately 2 km in diameter and has a maximum water depth of 34 m (Nakagawa et al., 2005).

In AD 1664, construction of a canal connecting Lake Suigetsu with Lake Kugushi (itself already connected to the sea) resulted in salt water inflow (Masuzawa & Kitano, 1982). The lake system is also fed with fresh water via the Hasu River, which flows into Lake Mikata, which in turn is connected to Lake Suigetsu by a shallow sill (<4 m water depth). As a result, Lake Suigetsu is today a meromictic lake with a chemocline between 3 and 8 m water depth, separating the lower salt water body and the upper fresh water layer (Kondo et al., 2009). Due to this artificial change in hydrology, most of the Lake Suigetsu sediments were deposited under limnological conditions that are only partially comparable to those of the present day.

Another effect of this particular setting is that Lake Mikata acts as a natural filter for coarse detrital material from the Hasu River catchment (Nakagawa et al., 2005), resulting in sedimentation of predominantly autochthonous and authigenic material in Lake Suigetsu. (Note that we use the term 'detrital' in its geologic meaning referring to weathered and eroded mineral matter.)

The sediments of the LGIT from Lake Suigetsu (core SG06) were described in detail by Schlolaut et al. (2012). They consist primarily of amorphous organic material, diatom frustules and Mn-enriched siderite ($[Fe,Mn]CO_3$), complemented by detrital grains and clay. All of these components formed seasonal layers in the sediment, but not consistently each year.

2. Materials and Methods

2.1 Core sampling and method overview

The SG06 composite core (Nakagawa et al., 2012) was constructed from sediment cores retrieved from four boreholes (A, B, C, D). Cores were split into halves (N, S) and digital core photographs were taken directly after core opening in the field, before colour changes due to oxidation could occur. The pictures were taken under natural daylight and include a scale and a colour chart. The core halves were then sampled with overlapping LL-channels, usually 1 m long. When two overlapping LL-channels were taken from a core, as was commonly the case, the channels were labelled upper and lower. With core number and 'SG06' for the project the complete labelling of an LL-channel is, for example, SG06-B(N)08 upper. LL-channels were then sent to the various participating laboratories for analysis.

The complete SG06 composite sediment core is 73.19 m long. The composite model used here is version '24Aug2009' and the interval from 1288 cm to 4040.8 cm composite depth (cd) is analysed in detail. Varve counting was carried out using a dual method approach utilising light microscopy and µXRF measurements independently. The data from these methods were also used for (micro)facies analysis alongside core photographs. Since seasonal layers did not form every year, or were not preserved, the varve counts were interpolated using the Varve Interpolation Program 3.0.0. For comparison the modelled $SG06_{2012}$ calendar chronology was used. These methods and data are explained in detail below.

2.2 Thin section microscopy

Varves were counted and measured using a petrographic microscope equipped with a calibrated ocular micrometer, at magnifications from 25× to 400×. Thickness and position measurements were made mainly at 25×. The standard reading error is 0.04 mm (i.e. one micrometer scale unit), although the uncertainty may be slightly higher in the case of diffuse layers or layers with variable thickness. Layers were assigned a quality from 1 (excellent) to 4 (poor) and, similarly, core intervals were assigned a quality score based on the quality of varve occurrence from 1 (perfectly varved) to 4 (poorly or not varved). This information was used to create 'quality selective datasets' for interpolation (see also section *3.2.1 Count datasets*).

2.3 µXRF core scanning

For µXRF-based varve counting, continuous measurements were made with an Itrax® core scanner on the sediment in LL-channels. For the Suigetsu sediment a 4.0 × 0.1 mm rectangular X-ray beam was used, with a step-size of 60 µm, a count time of 4 s, a voltage of 30 kV, a current of 30 mA and a Mo X-ray tube. Peaks interpreted to relate to seasonal layers were assigned a quality from 1 (excellent) to 4 (poor) for the creation of quality selective varve counts. A more detailed description of the settings used, as well as on the counting approach, is given by Marshall et al. (2012).

Due to the low count time of 4 s, only heavy or highly concentrated elements can be detected reliably, i.e. do not contain frequent null measurements. These are K, Ti, Fe, Mn and Zr. Ca is also considered. While Ca does contain null values, primarily in facies zone II, the overall percentage of these null values is only 0.13%.

The µXRF measurements of some LL-channels gave much higher intensities than measurements from parallel cores or even parallel channels from the same core (Fig. 2a). A particular reason for this offset could not be determined. Normalisation with incoherent scatter does not solve the issue (Fig. 2b). However, element ratios, such as K/Ti or K/Ca, negate the different intensities, as is evidenced by similar ratios in parallel core segments. Furthermore, only a few LL-channels are affected, all of which are from the LGIT section of the core (cores A7, B7, A8, B8, A9 lower, but not A9 middle nor A9 upper). Using the overlap of the cores, corrections for these measurements were calculated, assuming that overlapping core segments should have the same mean intensity for every element. For this a correction factor was calculated, being the mean intensity of the reference core divided by the mean intensity of core to be corrected. After correction the corrected core segment became the reference core for the next segment. We used core B(N)9 upper as the initial reference core, since it was the closest core segment to the above mentioned cores, which was not affected by any obvious offsets (Fig. 2c). This correction approach requires that the inter-core variability of the element signals is low, i.e. on a cm-scale the signals from overlapping cores are similar in shape and that there is sufficient overlap. We consider the correction reliable if after the correction the mean shape and magnitude, overall and local, of the curves are similar. The approach works well with K, Ca, Ti and Zr. Fe and Mn have in some core intervals a higher inter-core variability, introducing a degree of uncertainty. Furthermore, between the LL-channels B(N)8 upper and A(N)9 middle there is only a short overlap of 7 cm (ca. 1593 to 1600 cm cd), also introducing some uncertainty. However, the correction factors derived for B(N)8 upper are similar to the factors of B(S)8 lower and between these core segments is no apparent offset in the raw signal. Thus we judge the uncertainty deriving from the small overlap as low.

2.4 Varve interpolation

Since seasonal layers did not form in every year, or were not preserved, the varve record is incomplete and has been interpolated using the Varve Interpolation Program (VIP) 3.0.0

(Schlolaut, 2018) – an advanced version of the original VIP 1.0.0 (Schlolaut et al., 2012). The old VIP derived an estimate of the mean sedimentation rate (SR), which was then used for interpolation by determining if count distances are multiples of the mean SR. Count distances are the distances between seasonal layers, which are used for varve counting. In the case of Suigetsu these are usually the distances between autumn related siderite layers. The new program estimates the varve thickness frequency distribution and uses it for interpolation. The distribution is derived from Monte-Carlo distribution fitting to count distance frequency distributions. For fitting the count is divided into sub-sections and for every sub-section the fitting and interpolation is carried out independently. The program offers the possibility to adjust settings, controlling sub-section lengths, for example. The settings used here are listed and briefly explained in section *3.2.2 Interpolation*, after the results of the microfacies analysis have been presented, which influence our selection of the settings.

2.5 Modelled SG06$_{2012}$ chronology

The calendar chronology released in 2012 (Bronk Ramsey et al., 2012), to which we will refer as '(modelled) SG06$_{2012}$ chronology', is used here for comparison. Explicitly, it is used for comparison only and does not influence the creation of the new 2018 varve based chronology in any way. The modelled SG06$_{2012}$ chronology is underpinned by the 2012 varve based chronology, which uses the same varve count data from the dual method counting approach used here. However, the 2012 varve based chronology only reached back to ~40 ka BP, was extrapolated beyond this point and was interpolated using the VIP 1.0.0 rather than the VIP 3.0.0. To derive the SG06$_{2012}$ chronology the 2012 varve based chronology was constrained by the Bahamas speleothem GB89-25-3 (Hoffmann et al., 2010) and the Hulu Cave speleothem H82 (Southon et al., 2012) U-Th chronologies, using the low frequency $\Delta^{14}C$ signal from Lake Suigetsu and the speleothems to link the chronologies and improve precision and accuracy of the Suigetsu calendar chronology (Bronk Ramsey et al., 2012).

3. Results

3.1 Sedimentology

3.1 Sedimentology

The analysed interval, from 1288 to 4040.8 cm cd, corresponding roughly to the time window from 10 to 50 ka BP (Table 1), can be separated into three facies zones, labelled I to III from top to bottom, and several major microfacies zones (Fig. 3). Below 4040.8 cm cd lies facies zone IV, which is also briefly described here, though analysis was limited to 4500 cm cd. The sedimentological changes are presented in chronological order. Depths of microfacies zones are provided in table 1.

The sediment of **facies zone IV** (>4040,8 cm cd) is rich in clay and has the highest K intensity in the raw µXRF signal, as well as the highest mean K/Ti ratio (Fig. 4), indicative of a small grain size (Cuven et al., 2010). Variations in clay content produce mm to cm scale laminations evident in core photographs (Fig. 5). Seasonal siderite layers occur only infrequently with the minimum frequency of 0 layers per 10 cm being reached on more than one occasion. Therefore, microscopic analysis was not extended into this facies zone.

Facies zone III (4040.8 to 3095.9 cm cd) is characterised by a clay-rich matrix, a very high frequency of seasonal siderite layers and a high frequency of seasonal detrital layers. The detrital material is coarser than in the adjacent facies zones, which is for example reflected in low K/Ti and K/Ca ratios (Fig. 4). In Lake Suigetsu Ca is primarily associated with coarser grain sizes (Schlolaut et al., 2014) and tephra material. The varve structure (Fig. 7a,c) consists of a clay layer slightly enriched in organic material (winter or spring), a graded detrital layer interpreted to relate to the rainy season (summer), a siderite layer (autumn) and another graded detrital layer relating to the typhoon season (autumn), which in comparison to the rainy season layer is usually more enriched in clay. Associated with the second (autumn) detrital layer an additional siderite layer can occur, either within the detrital layer or towards the top where the clay fades into the more organic-rich layer.

Facies zone III can be divided into four microfacies zones. Microfacies zone III.d shows a very sudden onset of continuous siderite formation in the form of seasonal siderite layers and diffuse siderite. However, layer and lamination quality is relatively poor (Fig. 3,8) since it is difficult to distinguish the seasonal siderite layers in the generally siderite-rich sediment. Microfacies zone III.c is characterised by a very good lamination quality (Fig. 3,6,8). Visually it appears perfectly varved for the most part. In microfacies zone III.b the lamination quality decreases from the ‘excellent’ quality of microfacies zone III.c to a ‘very good’ and eventually to a 'good' quality – the sediment still appears largely varved, but cm to dm scale intervals occur in which siderite layers in particular become more diffuse, laterally variable to the point of discontinuous and/or did not form every year (Fig. 6). The onset of microfacies zone III.a is marked by a disturbance in the sediment (Fig. 5). The microfacies zone is ca. 25 cm long and the lamination is slightly disturbed, though still distinguishable. Seasonal layers show small folds and bends on mm to cm scale and have a higher lateral variability in their characteristics such as thickness (Figs. 5,6). This interval is topped by a massive event layer (3107 to 3095.9 cm cd), which also marks the boundary to facies zone II. Schlolaut et al., (2014) interpreted this event layer, denoted EL-3107, to be the result of a landslide into the lake, likely caused by an earthquake.

Facies zones II and I both have a much lower proportion of detrital material with a smaller grain size compared to facies zone III. This is apparent in thin sections and in the increase of the K/Ti and K/Ca ratios (Figs. 3,4). Furthermore, facies zones I and II also contain a higher proportion of organic material (Fig 8), mainly consisting of amorphous organic material and diatoms such as *Stephanodiscus*, *Aulacoseira* and *Chrysophyceae* cysts. The two facie zones also have a similar varve structure (Fig. 7b,d), described in detail by Schlolaut et al. (2012). It consists chiefly of a spring-related *Aulacoseira spp.* Layer (only in facies zone I), a spring-related siderite layer, a summer-related LAO layer, an autumn-related siderite layer and a typhoon season-related clay or graded detrital layer.

In addition to the description above, **Facies zone II** (3095.9 to 1728.5 cm cd) is also characterised by a generally poor lamination quality. It can be divided into three types of microfacies zones. In microfacies zone II.c the layer and lamination quality is better than in the younger sediment of facies zone II, but decreasing (Fig. 3). Microfacies zone II.a is interrupted by microfacies zone II.b, for which reason we distinguish between II.a1 (upper) and II.a2 (lower). The lamination quality in microfacies zone II.a is generally very poor. Seasonal siderite layers are separated by mm to cm scale homogenous layers, dominated by organic material, with diffuse siderite and detrital material. Microfacies zone II.b is characterised by an increased proportion of tephra material following the deposition of the AT-tephra. The boundaries of this microfacies zone are determined by the lower K/Ca and Ti/Ca ratio, reflecting the higher Ca content in the tephra material.

Particularly important for varve counting and interpolation are three intervals with anomalous characteristics within facies zone II. We will refer to these as ANI (ANomalous Interval) I to III.

For facies zone II these are unusually well laminated. This can be easily seen in figure 3 as an increase in LAO layer frequency as well as in siderite layer frequency. Additionally, ANI II and III are also characterised by an anomalously low sedimentation rate (SR), being less than half the average SR, reaching values as low as 0.2 mm/yr. These values are unique in the core interval analysed here. The low SR appears to be primarily due to a reduction in organic material (other than LAO layers) including diatoms.

Facies zone I (<1728.5 cm cd (analysed here to 1288 cm cd)) comprises the LGIT (I.d to I.b) and (early) Holocene (I.a). It is characterised by a further increased proportion of organic material, in particular diatoms. The lamination quality is clearly improved compared to facies zone II and well or even perfectly varved intervals are common. However, these are relatively short and of cm scale. As said and described above, the varve structure is very similar to that of facies zone II, though seasonal diatom layers are more common.

Facies zone I can be divided into four microfacies zones. The characteristics of the first microfacies zone, I.d, essentially match the general description of facies zone I. Microfacies zone II.c occurs after a 5.6 cm thick earthquake layer (Schlolaut et al., 2014) and is characterised by a high proportion of fine grained, diffuse detrital material and unusually massive siderite aggregates (Fig. 6,8). These make it harder to reliably distinguish seasonal siderite layers. Furthermore, the otherwise common seasonal layers of *Aulacoseira spp.* and LAO layers are absent in this interval. The next microfacies zone, I.b, is characterised by the best lamination quality within zone I. The onset of microfacies zone I.a marks the Holocene onset. The microfacies zone is characterised by a decrease in lamination quality. LAO and *Aulacoseira spp.* layers become uncommon and the siderite layer frequency is reduced compared to the previous microfacies zone (Fig. 3). The analysis described here does not extend above the U-Oki tephra at 1288 cm cd.

3.2 Varve age model

3.2.1 Count datasets

Both count datasets (microscope and µXRF) are based primarily on the counting of siderite layers. In the µXRF dataset these are distinguishable as peaks in Fe and Mn (Marshall et al., 2012). In the case of the microscope count, other seasonal layers, such as autumn-related detrital layers or the top of summer-related LAO layers, were also counted if siderite layers were absent.

Since seasonal layers did not form every year, or were not preserved, the Suigetsu varve chronology requires interpolation. Following the strategy of Schlolaut et al. (2012) and Marshall et al. (2012), quality selective datasets are used in addition to the complete (RAW) datasets. By "quality selective" we mean that count data of poor quality, e.g. due to low quality seasonal layers, were excluded. While this reduces the available information for interpolation it also reduces the amount of noise in the dataset. In the case of the microscope count a 'layer quality selective' (LQS) count was created, excluding counts that are based on layers which are difficult to measure as they are, for instance, diffuse, indistinct or laterally variable. Additionally a 'section quality selective' (SQS) dataset was created including only counts from relatively well varved intervals, i.e. not necessarily completely varved but with a regular lamination in which varves (seasonal layers that are one year apart) appear to dominate by at least 80% to 90%. Figure 3a shows the frequency of siderite layers of relatively good quality (quality 1 to 3), approximately equivalent to the LQS dataset, while figure 3b shows the frequency of low quality siderite layers (quality 4), which is approximately the difference between the RAW and LQS dataset. Figure 3e shows the frequency of relatively well varved intervals (quality 1 to 3). From the complete µXRF count only one quality selective dataset was created, which is 'peak quality selective', i.e. analogous to the LQS dataset. The complete µXRF dataset is labelled 'XQ4' as it includes all peak qualities from one to four, while the quality selective dataset is labelled 'XQ3'. Details on the definition of the peak quality can be found in Marshall et al. (2012). The quality determinations were made manually during varve counting and are therefore subjective to some degree.

Thus, there is a total of five count datasets available for interpolation (RAW, LQS, SQS, XQ4, XQ3) and ideally all should produce the same or similar interpolation results, given that they are all derived from the same composite sediment core (SG06). Differences allow us to identify and locate issues with the datasets and/or the interpolation, and evaluate these issues; for example by analysing count distance frequency plots (Schlolaut, 2018).

Note that the count datasets used here are the same as were used for the 2012 varve based model from the top of the varve counted interval at 1288 cm cd down to 3167.4 cm cd. Below this point the varve count data have now been extended to the facies III/IV boundary at 4040.8 cm cd.

3.2.2 Interpolation

Within the VIP 3.0.0 multiple parameters can be adjusted to improve the interpolation result. Information on the parameters and their impact on the interpolation is given in detail by Schlolaut (in press). Here, we briefly describe the parameters and explain which parameter values we used for the Suigetsu count data.

Firstly, sudden and large changes in SR are problematic for the VIP and there is the possibility that such changes are not placed correctly. This can be solved by using breakpoints at positions where such SR changes are particularly likely to occur, i.e. (micro)facies boundaries. Breakpoints essentially ensure that intervals separated by breakpoints are interpolated entirely independently. Therefore, we used all (micro)facies boundaries as described in section *3.1 Sedimentology* as breakpoints. Additionally, a breakpoint was defined at 1842.5 cm cd since the modelled 2012 chronology (Bronk Ramsey et al., 2012) suggests a change in SR at that point.

Secondly, we determined the most suitable σ range for the Monte-Carlo fitting of the varve thickness frequency distribution, since a narrower range improves the fitting. For that a run of the complete dataset with standard settings was performed. The result showed that the mean σ value of the varve thickness frequency distribution is relatively constant at about 0.34. Therefore, all subsequent calculations were made with a σ range of 0.25 to 0.4.

Since the mean SR should ideally be approximately constant for interpolation it is necessary to divide the count into shorter sub-sections that are more likely to meet this criterion. The sub-section length depends on the number of counts, that have a relatively small count distance to one another, i.e. are likely varves. The number of counts which need to be contained is given by the length control parameter. For the facies zones I and III we used relatively small subsection length control parameters (10, 12, 14, 16, 18, 20), producing rather short sub-sections. For facies zone II we used larger values (15, 20, 25, 30) since the generally poor lamination quality produces higher noise levels which make misfits in the fitting process more likely when short sub-sections are used. Longer sub-sections improve the signal to noise ratio. Furthermore, small, intermediate and large overlaps of the sub-sections were used (0.2, 0.5, 0.99).

The parameter ‘tolerance’ controls whether the program operates with a fit priority (large values) or with an ‘optimisation priority’ (small values). The program executes an optimisation loop, which aims to ensure that the SR of the interpolation result is the same as or sufficiently similar to the SR suggested by the estimated varve thickness frequency distribution. Here, we used small tolerance values (0, 1.25), i.e. not a fit priority, since the count data are noisy which increases the risk of misfits.

3.2.2.1 µXRF count and interpolation result

Marshall et al. (2012) showed that there are systematic differences between the quality selective µXRF count datasets, as well as between their interpolation results. The interpolation of the XQ3 count dataset gives systematically younger ages than XQ4. The extended results show that this is true for the complete sequence and persists with the VIP 3.0.0 (Fig. 9c). Marshall et al. (2012) also showed that neither count dataset is ‘wrong’ or ‘right’ per se. On the one hand XQ4 contains noise, i.e. counted non-seasonal peaks, and subsequently results in an over-count, in particular in well varved intervals. On the other hand, low quality or closely spaced siderite layers produce low quality peaks, which are not included in XQ3 – a problem particularly in facies zone II, which contains the lowest SRs and has the poorest lamination quality. Furthermore, this means that generally thin varves are underrepresented in XQ3. The extended dataset reveals that varves thinner than ~0.4 mm cannot be distinguished reliably in any of the µXRF count datasets, explicitly also not in XQ4. This is particularly apparent in the ANIs II and III in facies zone II. But the problem is not limited to intervals with a mean SR under 0.4 mm/a. Such thin varves are likely to also occur in intervals with a higher mean SR, e.g. 0.6 mm/a. Hence, in either dataset thin varves will be systematically underrepresented when the distance between siderite layers becomes small. Thus, intervals with rather thick siderite layers may also show systematic errors even if the mean SR is larger than the threshold. Since it cannot be said in which core intervals these issues occur without invoking other chronological data, the interpolated µXRF count cannot be used as a standalone dataset.

Compared to the 2012 interpolation results of the µXRF counts, the VIP 3.0.0 produces younger ages (XQ4: -3%, XQ3: -7%), with the difference being largest in facies zone II. The reason for this is that in the VIP 1.0.0 any count distance larger than 1.5 times the estimated mean SR was interpolated, which can lead to over-interpolation especially if the varve record is complete, or almost complete, requiring no or little interpolation. In contrast, the VIP 3.0.0 and the frequency distribution fitting approach allows for varves thicker than 1.5 times the mean SR.

3.2.2.2 Microscope count and interpolation result

The interpolation results from the different quality selective microscope counts show no systematic offset and agree remarkably well with one another (Fig. 9b). In some intervals, such as facies zone III.c, this is due to very similar datasets, since from a well varved raw count only few or no data are removed when creating a quality selective dataset. The comparison with the 2012 results based on the VIP 1.0.0 (Schlolaut et al., 2012, Bronk Ramsey et al., 2012) shows that the spread between the quality selective datasets is substantially reduced (Figs. 9a,b). For example, the maximum offset between the interpolated RAW and LQS datasets was 11% using the VIP 1.0.0. With the VIP 3.0.0 the maximum offset is reduced to -2%.

However, there are also some distinct differences between the interpolation results. In particular the interpolated SQS model diverges from the other two (Fig. 9d), which is most pronounced between the ANIs I and III (ca. +2000 yr) and in microfacieszone III.b (ca. -1500 yr). In the first case it must be considered that well laminated intervals are scarce and mainly near the ANIs (Fig. 3), which have lower than average SRs. Thus, it appears that the SRs in well laminated intervals are generally lower than in intervals with a poor lamination quality. Conversely, in the second case, i.e. microfacies zone III.b, well laminated intervals appear to occur under conditions that are associated with higher SRs. This illustrates that the conventional interpolation approach of using the SR of well varved intervals to interpolate non- or poorly varved intervals (e.g. Brauer et al, 1999, Hughen et al., 2004, Lauterbach et al. 2011) is not applicable to Lake Suigetsu.

3.2.2.3 Combining interpolation results into finalised 2018 varve based chronology

In order to combine the interpolation results from the different quality selective counts and the different settings used in the interpolation (such as sub-section length, overlap etc.) into a single finalised age model, the modal sedimentation rate per 5 cm from the individual models was used (Fig. 9e). The error estimates are given by the envelope of the individual age models

(Fig. 9e). Since SQS data are rather scarce, especially in facies zone II (Fig. 3), the different settings have little effect since sub-sections will reach from one breakpoint to another regardless of the setting. Hence, the SQS interpolation results are very similar and would thus dominate the combination of age models. To counter that only the SQS interpolation results from the two most different settings were considered and the modal value in the combination needs to be supported by at least five models.

Given the systematic uncertainties of the µXRF counts, these were excluded from the combination but are used for comparison in the next step.

The combination result, i.e. the finalised 2018 varve based chronology, with interpolation error estimates is shown in Figs. 9e,f. The precision of the age model is +8.9% and -4.6% relative to the varve dated interval, with on average 50% of the counts being interpolated relative to the RAW count, in facies zone II even up to an average of 70% of the counts (Fig. 10a). The chronology is anchored to a marker layer at 1397.4 cm cd, which has been dated by Staff et al. (2013) to 11,241 ± 17 cal yr BP (mean ± 1 sigma value; 11,275 to 11,209 cal yr BP 95.4% probability range). The uncertainty of the anchored chronology relative to the calendar age is +7.1% and -3.7%. Comparison with the interpolated µXRF counts (XQ3, XQ4) shows that both µXRF models show large offsets from the combination result, but that interval-wise for most parts either XQ3 (in intervals with a relatively high SR) or XQ4 (in intervals with a low SR) do agree relatively well with combination result (Fig. 9g). The most notable exception is the ANI III with the SR being clearly below the methodological limit of either µXRF count. Furthermore, the combination result does agree rather well with the 2012 RAW interpolation result in the common interval (Fig. 9f).

4. Discussion

4.1. (Micro)facies changes and chronology

With respect to the interpolation of the count datasets, facies zone III.a and its relation to the event layer EL-3107 immediately above it must be discussed in more detail. Schlolaut et al. (2014) argued that EL-3107 is indicative of an earthquake, which also resulted in the re-routing of the Hasu River to Lake Mikata, while the river previously entered Lake Suigetsu more directly via Lake Suga. The results presented here support this theory. The higher proportion of detrital material, the larger grain size and the occurrence of rainy season (summer) related detrital layers during facies zone III suggest that the present day filter function of Lake Mikata was not active at the time. The characteristics of microfacies zone III.a, i.e. small folds and bends suggesting movement of the sediment, and the distinct base, raise the question of whether III.a is part of the event layer, i.e. that it represents a slump caused by the earthquake. In this case varve interpolation within III.a would lead to erroneously old varve ages for the sediments below this point. We argue that III.a is not a slump for the following reasons. Firstly, the lamination of this interval is horizontally aligned, which makes a displacement from the steep lake slopes unlikely. In contrast to the lake slopes the lake bottom is very flat (~5 m of depth change occur along ~600 m, i.e. a slope of 0.8%) and thus unfavourable for slumps. Secondly, the same microfacies zone can be observed in the new 'SG14' sediment core retrieved circa 330 m to the east of the SG06 drilling location. The thickness difference SG14 minus SG06 of zone III.a is 8 mm (3%), which is well within the natural sediment accumulation variability of these two locations. This means that if the sediment of zone III.a had been displaced it would have covered the lake floor in a rather unexpected uniform and large scale fashion. There are also no indications of an age reversal in ^{14}C dates from this microfacies zone, but since it lies at the edge of a ^{14}C plateau, this cannot be used as conclusive evidence in itself.

Another chronological issue relating to microfacies changes is in the aftermath of the AT-tephra deposition, i.e. microfacies zone II.b, in which the sediment is clearly enriched in tephra material. The microfacies zone shows a relatively good lamination quality, especially at its base, consisting of graded detrital layers (Fig. 8) and after circa 10 cm also siderite layers (Fig. 6). The siderite layers suggest that the graded detrital layers are of annual origin, rather than being the result of individual, strong rain events, which may occur multiple times in a year. However, since no siderite layers occur in the first 10 cm an over-count cannot be ruled out, given that there is no independent proof that all of the detrital layers are indeed annual.

With respect to the interpolation results from the different facies zones we find that the interpolation error estimates are higher in facies zones I (+11.3%, -8.1%) and III (+14.1%, -1.9%) compared to facies zone II (5.9%, -5.8%), despite the latter having the poorest lamination quality. This is due to a higher mean SR variability in facies zones I and III. Facies zone I, comprising the LGIT and early Holocene, was affected by a highly unstable climate, which resulted in variable SRs. Furthermore, there are indications for local events impacting the lake. The most prominent example for this is microfacies zone I.c, which appears to be related to a lake level change as a result of the earthquake, which produced the underlying event layer EL-1632.6 (Fig. 3). In facies zone III the higher variability in mean SR is related to a higher sensitivity of the sediment to centennial scale climate cycles. These cycles can, for example, be observed in typhoon layer frequency. For the interpolation this means that mean SR changes occur more frequently within sub-sections, i.e. that the prerequisite of an approximately constant mean SR within sub-sections is more frequently not fulfilled. This will, for example, affect long sub-sections more often than short sub-sections. Thus, there will be a higher variability in interpolation results, since longer sub-sections are more likely to give different results from shorter sub-sections. In the combination of the interpolation results from the different quality selective counts and the different settings (Fig. 9e) the higher variability results in a higher interpolation error estimate. However, the similarity between the interpolated RAW and LQS datasets (Fig. 9b) indicates that this affects precision stronger than accuracy. The RAW dataset has systematically shorter sub-sections than the LQS dataset, since the former contains more counts, but there is no systematic offset between the interpolated RAW and LQS count.

4.2. Comparison with 2012 results

Here we compare the 2018 varve based chronology with the 2012 varve based chronology (Fig. 10b) as well as with the modelled and U-Th moderated $SG06_{2012}$ chronology (Fig. 9f).

We find that the 2012 and the 2018 varve based chronologies are extremely similar from the top (U-Oki tephra, 1288 cm cd) to 1980 cm cd and from the top of ANI III (2375 cm cd) to the bottom of the 2012 varve based chronology (3167 cm cd). The degree of similarity in these intervals is remarkable given that the interpolation approach is different, that the interpolation results of quality datasets are different and that µXRF results were not integrated into the new age model. However, between 1980 and 2375 cm cd, a large offset between the 2012 and 2018 varve based chronologies occurs (ca. 1650 yr). Since the varve model is cumulative from top to bottom, the offset does persist down-core. The difference is due to the integration of µXRF age models into the 2012 varve model. Specifically, in the 2012 varve model only XQ4 was used for the Glacial section, while XQ3 was only used in the LGIT and Holocene section. This pre-selection introduced a human bias, as it excluded the occurrence of larger SRs in the Glacial.

It is noteworthy that the upper error estimate of the 2018 varve based chronology approximately coincides with the 2012 varve model, while the 2018 varve based chronology broadly coincides with the lower error estimate of the 2012 varve model. This means that (i) the 2012 varve based chronology remains a valid result within error estimates and (ii) it indicates that the accurate result likely lies between the 2018 varve based chronology and its upper error estimate.

Compared to the modelled $SG06_{2012}$ chronology we find a similar offset as in the comparison between the 2012 and 2018 varve based chronologies, but the divergence starts further up-core, at the boundary between facies zone I and II. This means that the new 2018 varve based chronology does not support the divergence the modelling produced from the 2012 varve model between ca. 1730 and 1850 cm cd. Furthermore, the 2018 varve based chronology, in terms of mean SR, also diverges in facies zone III from the modelled $SG06_{2012}$ chronology. All interpolated quality selective models from the microscope count as well as the combined model suggest a higher mean SR. However, a divergence in facies zone III is less surprising, considering that the $SG06_{2012}$ chronology used a linearly extrapolated varve age model beyond 3167 cm cd.

4.3 Comparison with other varve chronologies

Compared to other varve chronologies the varve based 2018 Suigetsu chronology is unique in two ways. Firstly, it is by far the longest continuous chronology based on varve dating. The varve dated interval spans approximately 38,000 years. The second longest varve chronology listed in the Varve Data Base (VDB) (Ojala et al., 2012) is the Holzmaar chronology (Zolitschka et al., 2000), covering circa 23,000 years, and the third longest is the Cariaco Basin chronology (Hughen et al., 2000) with approximately 15,000 years. Secondly, the Suigetsu chronology relies very heavily on varve interpolation. For this reason it has a much higher age uncertainty than most varve chronologies. The VDB shows that 82% of the varve records published with a quantitative error estimate have an error of ≤4%, with a median of ~2%. However, comparing the uncertainties of varve chronologies is not straightforward since there is no standard procedure for error estimation. One common approach for estimating count uncertainties is the creation of replicated counts, i.e. counting of the same sediment by different individuals. While this allows estimation of the human bias and/or identification of core intervals with increased uncertainties due to poorly distinguishable varves, it cannot identify missing varves.

This can be partially countered by cross-dating, i.e. counting on parallel cores, which can be used to obtain a (minimum) estimate of missing counts (e.g. Mangili et al., 2005, Neugebauer et al., 2012). Brauer et al. (2001) compared LGIT climate boundaries determined by pollen analysis between the Holzmaar and Meerfelder Maar records, both of which are varved and which are <10 km apart from one another. Results showed that the dating differences ranged between -8% and 32% (Meerfelder Maar relative to Holzmaar) for the different climatic episodes during the LGIT. The original error estimate of the LGIT section of the Holzmaar chronology based on replicated counts was 6% (Zolitschka et al., 2000). The larger differences between the two records were not only due to varve count uncertainties, but also due to hiatuses, which could be identified by this cross-dating approach, and due to uncertainties in determining pollen boundaries, which are not always sharp. In the case of Lake Suigetsu the dual method counting approach was originally intended to identify/quantify varve count uncertainties. However, the sensitivities of the two approaches turned out to be too different to allow any meaningful comparison of the raw counts. The µXRF count identified circa twice as many counts, based upon counted element peaks interpreted to be seasonal signals compared to the microscope count (RAW) based upon visually identified seasonal layers. Nevertheless, the comparison enabled the identification of method related, systematic differences. Varve count uncertainties are represented to some degree in the quality selective datasets. However, especially with the microscope count, this does not solely reflect varve distinguishability but also count distance measurement uncertainty, due to, e.g., seasonal layers not being parallel or being diffuse. As discussed previously, the quality selective counts were specifically created to identify potential systematic impacts of count uncertainties on the interpolation.

Another approach to the estimation of varve count uncertainties is the comparison with results from other dating methods. For long varve chronologies ^{14}C dating is most commonly used. If large differences are identified the dating results are often also used to correct the varve count. For instance, the ca. 14,000 year long Sihailongwan varve chronology (Schettler et al., 2006) showed a -6% difference to the ^{14}C chronology of the record and was eventually corrected by multiplication with a constant correction factor to account for the difference. In such instances it needs to be taken into consideration that the alternative dating method has uncertainties itself. Since the Suigetsu chronology is intended to contribute to ^{14}C calibration any consideration or incorporation of ^{14}C data would be circular and is therefore not an option.

However, if in the future independent tephra dates for the many tephras in the Lake Suigetsu sediment (Smith et al., 2013) could be obtained, these could be used to improve and/or constrain the error estimates of the varve based chronology.

In summary, the comparisons of error estimates between varve chronologies is difficult due to the different error estimation techniques used (if any – only 57% of the records in the VDB are published with quantitative error estimates) and due to the different types of errors – most prominently counting and interpolation errors. However, it is also clear that the heavily interpolated Suigetsu varve chronology cannot be as precise as an (almost) perfectly varved record. The interpolation error estimates of +8.9% and -4.6% are very good considering the high degree of interpolation and the length of the record, given that long records are less likely to be continuously perfectly or well varved. Furthermore, the error estimates are objectively derived without invoking any other dating method or climate tuning.

5. Conclusions

We have presented a detailed description of the microfacies changes in the Lake Suigetsu sediments from ~10 to ~50 ka BP. Microfacies analysis did not reveal any indication for hiatuses in the sediment. Lamination quality is relatively good in the top (facies zone I) and bottom (facies zone III), but rather poor in the middle interval (facies zone II) of the analysed core section. Seemingly perfect varve formation and preservation for an extended period of time only occurs at the bottom of facies zone III. Otherwise perfectly varved intervals usually only occur on a mm to cm scale. All facies zones require varve interpolation. The results presented here are extended by ~10 ka compared to the 2012 varve based chronology, and have been interpolated with a different method. The comparison between the old and new results allows us to better constrain the certainties and uncertainties related to varve counting and interpolation. With respect to varve counting, in particular the dual method counting approach, we can draw a number of conclusions. The counting by µXRF is in principle viable, which is shown by the fact that for the most part either the interpolated XQ4 or XQ3 dataset agrees with the interpolated microscope count. However, since very thin varves cannot be distinguished in the µXRF signal and because we have found systematic differences between XQ3 and XQ4, µXRF counting can only be used as a standalone approach under rather specific conditions, which are consistently thick varves relative to the applied resolution and beam size as well as low noise levels relative to the signals of seasonal layers. In cases of poor lamination quality µXRF counting can be a useful addition, but should be carried out alongside microscopic counting rather than independently, to utilise the maximum amount of information for the counting of each seasonal layer/signal. For such an approach it needs to be ensured that the same plane is measured that is visible in the thin section. Otherwise, small variations in layer thickness can make sub-mm alignment difficult over longer intervals. How measurement of the same plane can be achieved was described by Brauer et al. (2009).

With respect to the Suigetsu varve chronology we have shown that there is a high degree of similarity between the 2012 chronology and the chronology presented here from the top at 1288 cm cd to 1980 cm cd and between 2375 cm cd and the lower limit of the 2012 chronology at 3167.4 cm cd. The degree of similarity despite the very different processing of the counts suggests an accurate reconstruction of the SR in these intervals. However, in between, from 1980 to 2375 cm cd, we find a major divergence of ~1650 yr, though within error estimates. Due to the cumulative character of the varve count and the interpolation, this means that all absolute ages below this point are affected by this uncertainty. However, the agreement of reconstructed mean SRs below 2375 cm cd means that the chronology is well suited for differential dating in this interval. To improve the absolute ages, further age constraints would be necessary, for instance, by the approach that Bronk Ramsey et al. (2012) applied, constraining the varve ages by modelling radiocarbon with speleothem U-Th ages. Alternatively, if for certain horizons, such as tephra layers, independent absolute ages can be obtained in the future, these could be used to constrain the spread in the models from individual settings of the varve interpolation (Fig. 9e).

Acknowledgements

We thank the Japan Society for the Promotion of Science (JSPS KAKENHI grant JP15H06905, fellowship grant PE07622), the German Research Foundation (DFG grant BR 2208/7-1), the UK Natural Environment Research Council (NERC grants NE/D000289/1, NE/F003048/1, SM/1219.0407/001), and the Leverhulme Trust (grant ECF-2015-396).

References

Brauer, A., Endres, C., Negendank, J.F., 1999. Lateglacial calendar year chronology based on annually laminated sediments from Lake Meerfelder Maar, Germany. Quaternary International 61, 17 – 25.

Brauer, A., Litt, T., Negendank, J.F.W., Zolitschka, B. 2001. Lateglacial varve chronology and biostratigraphy of lakes Holzmaar and Meerfelder Maar, Germany. Boreas 30, 83 – 88.

Brauer, A., Dulski, P., Mangili, C., Mingram, J., Liu, J., 2009. The potential of varves in high-resolution paleolimnological studies. PAGES news 17, 96 – 98.

Bronk Ramsey, C., Lee, S., 2013. Recent and Planned Developments of the Program OxCal. Radiocarbon 55, 720-730

Bronk Ramsey, C., Staff, R.A., Bryant, C.L., Brock, F., Kitagawa, H., van der Plicht, J., Schlolaut, G., Marshall, M.H., Brauer, A., Lamb, H.F., Payne, R.L., Tarasov, P.E., Haraguchi, T., Gotanda, K., Yonenobu, H., Yokoyama, Y., Tada, R., Nakagawa, T., 2012. A Complete Terrestrial Radiocarbon Record for 11.2 to 52.8 kyr B.P. Science 338, 370–374.

Cuven, S., Francus, P., Lamourex S.F., 2010. Estimation of grain size variability with micro X-ray fluorescence in laminated lacustrine sediments, Cape Bounty, Canadian High Arctic. Journal of Paleolimnology 44, 803 – 817

Hoffmann, D.L., Beck, J.W., Richards, D.A., Smart, P.L., Singarayer, J.S., Ketchmark, T., Hawkesworth, C.J., 2010. Towards radiocarbon calibration beyond 28 ka using speleothems from the Bahamas. Earth and Planetary Science Letters 289, 1 – 10.

Hughen, K.A., Southon, J.R., Lehman, S., Overpeck, J., 2000. Synchronous radiocarbon and climate shifts during the last deglaciation. Science 290, 1951 – 1954.

Hughen, K.A., Southton, J.R., Bertrand, C.J.H., Frantz, B., Zermeño, P., 2004. Cariaco basin calibration update: revisions to calendar and 14C chronologies for core PL07-58PC. Radiocarbon 46, 1161 – 1187.

Katsuta, N., Takano, M., Kawakami, S.-I., Togami, S., Fukusawa, H., Kumazawa, M., Yasuda, Y., 2006. Climate system transition from glacial to interglacial state around the beginning of the last termination: Evidence from a centennial-to millennial-scale climate rhythm. Geochemistry Geophysics Geosystems 7.

Katsuta, N., Takano, M., Kawakami, S.-I., Togami, S., Fukusawa, H., Kumazawa, M., Yasuda, Y., 2007. Advanced Micro-XRF Method to Separate Sedimentary Rhythms and Event Layers in Sediments: Its Application to Lacustrine Sediment from Lake Suigetsu, Japan. Journal of Paleolimnology 37, 259–271.

Kitagawa, H., Fukuzawa, H., Nakamura, T., Okumura, M., Takemura, K., Hayashida, A., Yasuda, Y., 1995. AMS ^{14}C dating of varved sediments from Lake Suigetsu, Central Japan and atmospheric ^{14}C change during the Late Pleistocene. Radiocarbon 37, 371–378.

Kitagawa, H., van der Plicht, J., 1998. Atmospheric Radiocarbon Calibration to 45,000 yr B.P.: Late Glacial Fluctuations and Cosmogenic Isotope Production. Science 279, 1187 – 1190.

Kitagawa, H., van der Plicht, J., 2000. Atmospheric radiocarbon calibration beyond 11,900 cal BP from Lake Suigetsu laminated sediments. Radiocarbon 42, 369 – 380.

Kondo, R., Nakagawa, A., Mochizuki, L., Osawa, K., Fujioka, Y., Butani, J., 2009. Dominant bacterioplankton populations in the meromictic Lake Suigetsu as determined by denaturing gradient gel electrophoresis of 16S rRNA gene fragments. Limnology 10, 63–69.

Kossler, A., Tarasov, P., Schlolaut, G., Nakagawa, T., Marshall, M., Brauer, A., Staff, R., Bronk Ramsey, C., Bryant, C., Lamb, H., Demske, D., Gotanda, K., Haraguchi, T., Yokoyama, Y., Yonenobu, H., Tada, R., 2011. Onset and termination of the late-glacial climate reversal in the high-resolution diatom and sedimentary records from the annually laminated SG06 core from Lake Suigetsu, Japan. Palaeogeography, Palaeoclimatology, Palaeoecology 306, 103 – 115.

Lauterbach, S., Brauer, A., Andersen, N., Danielopol, D.L., Dulski, P., Hüls, M., Milecka, K., Namiotko, T., Obremska, M., von Grafenstein, U., Declakes Participants, 2011. Environmental responses to Lateglacial climatic fluctuations recorded in the sediments of pre-Alpine Lake Mondsee (northeastern Alps). Journal of Quaternary Science 26, 253 – 267.

Mangili, C., Brauer, A., Moscariello, A., Naumann, R., 2005. Microfacies of detrital event layers deposited in Quaternary varved lake sediments of the Piànico-Sèllere Basin (northern Italy). Sedimentology 52, 927 – 943.

Marshall, M., Schlolaut, G., Brauer, A., Nakagawa, T., Staff, R.A., Bronk Ramsey, C., Lamb, H., Gotanda, K., Haraguchi, T., Yokoyama, Y., Yonenobu, H., Tada, R., SG06 project members, 2012. A novel approach to varve counting using µXRF and X-radiography in combination with thin-section microscopy, applied to the Late Glacial chronology from Lake Suigetsu, Japan. Quaternary Geochronology 13, 70–80.

Masuzawa, T., Kitano, Y., 1982. Sulfate reduction and sulfur fixation in sediment of a historically meromictic lake, Lake Suigetsu, Japan. Journal of Oceanography 38, 21–27.

McLean, D., Albert, P.G., Nakagawa, T., Staff, R.A., Suzuki, T., Suigetsu 2006 Project Members, Smith, V.C., 2016. Identification of the Changbaishan 'Millennium' (B-Tm) eruption deposit in the Lake Suigetsu (SG06) sedimentary archive, Japan: Synchronisation of hemispheric-wide palaeoclimate archives. Quaternary Science Reviews 150, 301 – 307.

Nakagawa, T., Kitagawa, H., Yasuda, Y., Tarasov, P.E., , Nishida, K., Gotanda, K., Sawai, Y., 2003. Asynchronous Climate Changes in the North Atlantic and Japan During the Last Termination. Science 299, 688 – 691.

Nakagawa, T., Tarasov, P.E., Nishida, K., Gotanda, K., Yasuda, Y., 2002. Quantitative pollen-based climate reconstruction in central Japan: application to surface and Late Quaternary spectra. Quaternary Science Reviews 21, 2099 – 2113.

Nakagawa, T., Gotanda, K., Haraguchi, T., Danhara, T., Yonenobu, H., Brauer, A., Yokoyama, Y., Tada, R., Takemura, K., Staff, R.A., Payne, R., Bronk Ramsey, C., Bryant, C., Brock, F., Schlolaut, G., Marshall, M., Tarasov, P., Lamb, H., 2012. SG06, a fully continuous and varved sediment core from Lake Suigetsu, Japan: stratigraphy and potential for improving the radiocarbon calibration model and understanding of late Quaternary climate changes. Quaternary Science Reviews 36, 164 – 176.

Nakagawa, T., Kitagawa, H., Yasuda, Y., Tarasov, P.E., Gotanda, K., Sawai, Y., 2005. Pollen/event stratigraphy of the varved sediment of Lake Suigetsu, central Japan from 15,701 to 10,217 SG vyr BP (Suigetsu varve years before present): Description, interpretation, and correlation with other regions. Quaternary Science Reviews 24, 1691 – 1701.

Nakagawa, T., Tarasov, P.E., Kitagawa, H., Yasuda, Y., Gotanda, K., 2006. Seasonally specific responses of the East Asian monsoon to deglacial climate changes. Geology 34, 521 – 524.

Neugebauer, I., Brauer, A., Dräger, N., Dulski, P., Wulff, S., Plessen, B., Mingram, J., Herzschuh, U., Brande, A., 2012. A Younger Dryas varve chronology from the Rehwiese palaeolake record in NE-Germany. Quaternary Science Reviews 36, 91 – 102.

Ojala, A.E.K., Francus, P., Zolitschka, B., Besonen, M., Lamoureux, S.F., 2012. Characteristics of sedimentary varve chronologies – A review. Quaternary Science Reviews 43, 45 – 60.

Reimer, P., Bard, E., Bayliss, A., Beck, J., Blackwell, P., Bronk Ramsey, C., Buck, C., Cheng, H., Edwards, R., Friedrich, M., Grootes, P., Guilderson, T., Haflidason, H., Hajdas, I., Hatté, C., Heaton, T., Hoffmann, D., Hogg, A., Hughen, K., Kaiser, K., Kromer, B., Manning, S., Niu, M., Reimer, R., Richards, D., Scott, E., Southon, J., Staff, R., Turney, C., & van der Plicht, J., 2013. IntCal13 and Marine13 Radiocarbon Age Calibration Curves 0–50,000 Years cal BP. Radiocarbon, 55(4), 1869 – 1887.

Schettler, G., Liu, Q., Mingram, J., Stebich, M., Dulski, P., 2006. East-Asian monsoon variability between 15000 and 2000 cal. Yr BP recorded in varved sediments of Lake Sihailongwan (northeastern China, Long Gang volcanic field). The Holocene 16, 1043 – 1057.

Schlolaut, G., Marshall, M.H., Brauer, A., Nakagawa, T., Lamb, H.F., Staff, R.A., Bronk Ramsey, C., Bryant, C.L., Brock, F., Kossler, A., Tarasov, P.E., Yokoyama, Y., Tada, R., Haraguchi, T., Suigetsu 2006 project members, 2012. An automated method for varve interpolation and its application to the Late Glacial chronology from Lake Suigetsu, Japan. Quaternary Geochronology 13, 52–69.

Schlolaut, G., Brauer, A., Marshall, M.H., Nakagawa, T., Staff, R.A., Bronk Ramsey, C., Lamb, H.F., Bryant, C.L., Naumann, R., Dulski, P., Brock, F., Yokoyama, Y., Tada, R., Haraguchi, T., Suigetsu 2006 project members, 2014. Event layers in the Japanese Lake Suigetsu `SG06' sediment core: description, interpretation and climatic implications. Quaternary Science Reviews 83, 157 – 170.

Schlolaut, G., Brauer, A., Nakagawa, T., Lamb, H.F., Tyler, J.J, Staff, R.A., Marshall, M.H., Bronk Ramsey, C., Bryant, C.L., Tarasov, P.E., 2017. Evidence for a bi-partition of the Younger Dryas Stadial in East Asia associated with inversed climate characteristics compared to Europe. Scientific Reports 7, doi:10.1038/srep44983.

Schlolaut, G., 2018. The Varve Interpolation Program 3.0.0 - A unique and easy to use tool for incompletely varved sediments. Quaternary Geochronology 48, 17 – 24.

Smith, V.C., Staff, R.A., Blockley, S.P.E., Bronk Ramsey, C., Nakagawa, T., Mark, D.F., Takemura, K., Danhara, T., Suigetsu 2006 Project Members, 2013. Identification and correlation of visible tephras in the Lake Suigetsu SG06 sedimentary archive, Japan: chronostratigraphic markers for synchronising of east Asian/west Pacific palaeoclimatic records across the last 150 ka. Quaternary Science Reviews 67, 121 – 137.

Southon, J., Noronha, A.L., Cheng, H., Edwards, R.L., Wang, Y., 2012. A high-resolution record of atmospheric ^{14}C based on Hulu Cave speleothem H82. Quaternary Science Reviews 33, 32 – 41.

Staff, R.A., Bronk Ramsey, C., Nakagawa, T., Suigetsu 2006 project members, 2010. A re-analysis of the Lake Suigetsu terrestrial radiocarbon calibration dataset. Nuclear Instruments and Methods in Physics Research Section B: Beam Interactions with Materials and Atoms 268, 960 – 965.

Staff, R.A., Nakagawa, T., Schlolaut, G., Marshall, M.H., Brauer, A., Lamb, H., Bronk Ramsey, C., Bryant, C.L., Brock, F., Kitagawa, H., van der Plicht, J., Payne, R.L., Smith, V.C., Mark, D.F., MacLeod, A., Blockley, S.P.E., Schwenninger, J.L., Tarasov, P., Haraguchi, T., Gotanda, K., Yonenobu, H., Yokoyama, Y., Suigetsu 2006 project members, 2013. The Multiple Chronological Techniques Applied to the Lake Suigetsu (SG06) Sediment Core. Boreas 42, 1502 – 3885.

Tyler, J., Kashiyama, Y., Ohkouchi, N., Ogawa, N., Yokoyama, Y., Chikaraishi, Y., Staff, R.A., Ikehara, M., Bronk Ramsey, C., Bryant, C., Brock, F., Gotanda, K., Haraguchi, T., Yonenobu, H., Nakagawa, T., 2010. Tracking aquatic change using chlorine-specific carbon and nitrogen isotopes: The last glacial-interglacial transition at Lake Suigetsu, Japan. Geochemistry Geophysics Geosystems 11, doi:10.1029/2010GC003186.

Zolitschka, B., Brauer, A., Negendank, J.F.W., Stockhausen, H., Lang, A., 2000. Annually dated late Weichselian continental paleoclimate record from the Eifel, Germany. Geology 28, 783 – 786.

Figure Captions

Fig. 1

Location of Lake Suigetsu (modified after Nakagawa et al. (2012) and topographic map of the Geospatial Information Authority of Japan).

Fig. 2

Offset and subsequent correction of µXRF data from the LGIT shown on the example of Ti. Plots show 83 point (~5 mm) moving averages. (a) raw measurements (b) normalised with incoherent scatter (c) using correction factors to adjust mean intensities in overlapping intervals to a reference core

Fig. 3

Overview of facies and microfacies zones with selected proxy data: (a) frequency of readily distinguishable siderite layers (quality 3 or better), (b) frequency of low quality siderite layers, (c) frequency of LAO layers, (d) µXRF K/Ca ratio (red line is the 833 point (~5 cm) moving average) and (e) manually determined lamination quality score. For the definition of facies boundaries and a discussion of the data refer to the main text.

Fig. 4

Overview µXRF data. Red curves show the 833 point (~5 cm) moving average. Y-axis labels marked with '*' mean that the data were corrected at the top (see Fig. 2 and section *2.3 µXRF core scanning*).

Fig. 5

Core photographs of the three facies boundaries (IV to III, III to II and II to I).

Fig. 6

Examples of thin section scans in polarised light from the different microfacies zones. Yellowish layers consist of siderite.

Fig. 7

(a)Idealised varve structure of facies zone III, (b) idealised varve structure of facies zone I (Schlolaut et al., 2012), which is in principle also applicable to facies zone II, though in facies zone II only siderite, LAO and graded detrital layers were observed, (c) microscope photos of varves in facies zone III, (d) microscope photos of varves in facies zone I

Fig. 8

Examples of microscope photographs from selected microfacies zones. Note that all photographs have the same scale and were taken under identical light conditions.

Fig. 9

Comparison of different age depth models: (a) shows the relatively strong spread between the interpolated 2012 quality selective microscope age models and in comparison (b) shows the clearly improved agreement of the 2018 quality selective microscope age models; (c) shows the systematic offset between the two interpolated quality selective µXRF counts; (d) shows the differences between the interpolated 2018 quality selective microscope age models – horizontal intervals of the curves indicate a good agreement; (e) shows the results of the interpolation for each setting of the VIP 3.0.0 (grey) and the combination result (red), i.e. the 2018 varve based chronology; (f) shows the modelled $SG06_{2012}$ chronology (green) with 2018 varve based chronology (red); (g) shows the difference plots of the 2018 varve based chronology and the quality selective µXRF varve models; (h) shows the good agreement between the 2018 varve based chronology and the 2012 interpolated RAW count. The transparent background colours indicate the different microfacies zones (see Fig. 3); on the right side a colour legend for the microfacies zones is provided. *EL* stands for Event Layer and *T* stands for Tephra; with only those mentioned in the text being shown.

Fig. 10

(a) Percentage of counts interpolated in the 2018 varve based chronology relative to the microscope RAW count. (b) Comparison of 2018 with the 2012 varve based model, showing that the 2018 varve based model approximately coincides with the lower error estimate of the 2012 model, while the upper error of the 2018 model coincides with the 2012 model. The transparent background colours indicate the different microfacies zones (see Fig. 3); on the right side a colour legend for the microfacies zones is provided. *EL* stands for Event Layer and *T* stands for Tephra; with only those mentioned in the text being shown.

Table Captions

Table 1

Ages of facies and microfacies boundaries. The ^{14}C chronology has been calibrated with IntCal13 (Reimer et al., 2013) and modelled with OxCal (Bronk Ramsey & Lee, 2013). The unit 'vyr' stands for 'varve years' and B.P. refers to A.D. 1950 in all age models.

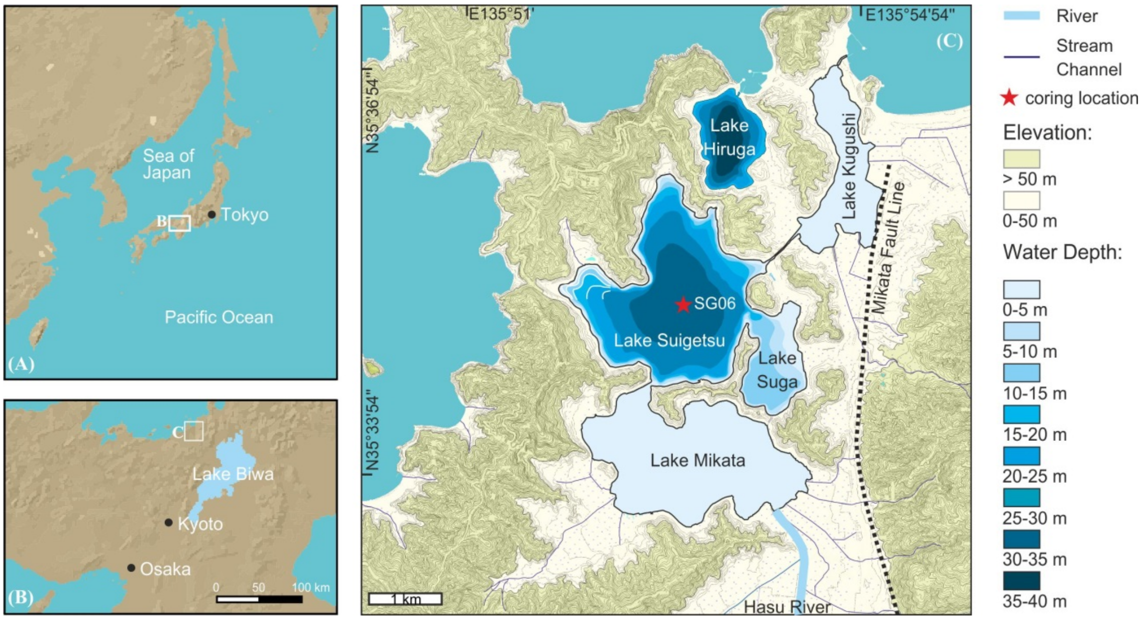
Sea of Japan
Tokyo
B
Pacific Ocean
(A)
C
Lake Biwa
Kyoto
Osaka
0 50 100 km
(B)
E135°51'
E135°54'54"
(C)
N35°36'54"
N35°33'54"
Lake Hiruga
Lake Kugushi
Mikata Fault Line
SG06
Lake Suigetsu
Lake Suga
Lake Mikata
1 km
Hasu River
River
Stream Channel
coring location
Elevation:
> 50 m
0-50 m
Water Depth:
0-5 m
5-10 m
10-15 m
15-20 m
20-25 m
25-30 m
30-35 m
35-40 m

895 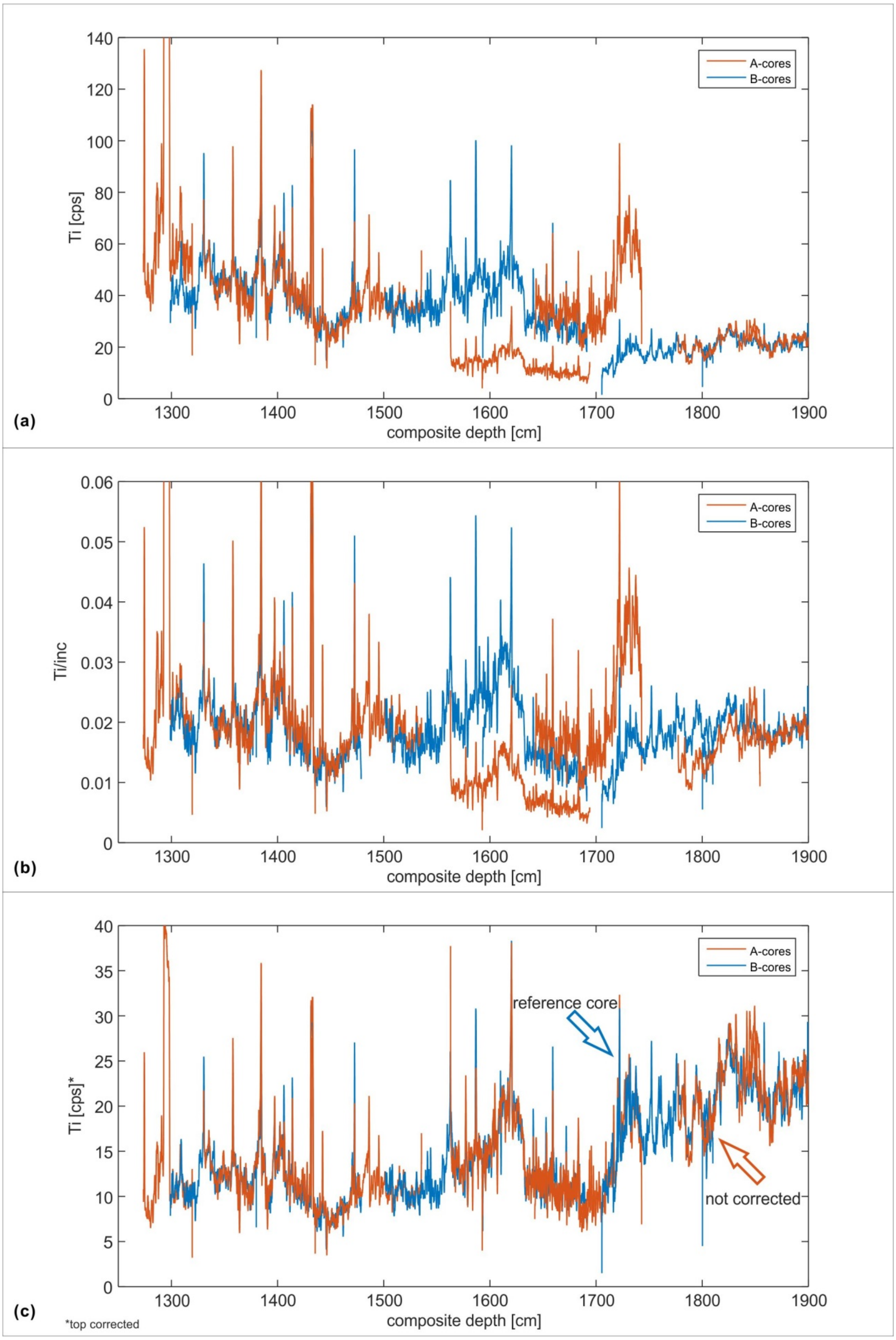

Ti [cps]
A-cores
B-cores
(a)
composite depth [cm]
Ti/inc
A-cores
B-cores
(b)
composite depth [cm]
Ti [cps]*
A-cores
B-cores
reference core
not corrected
(c)
*top corrected
composite depth [cm]

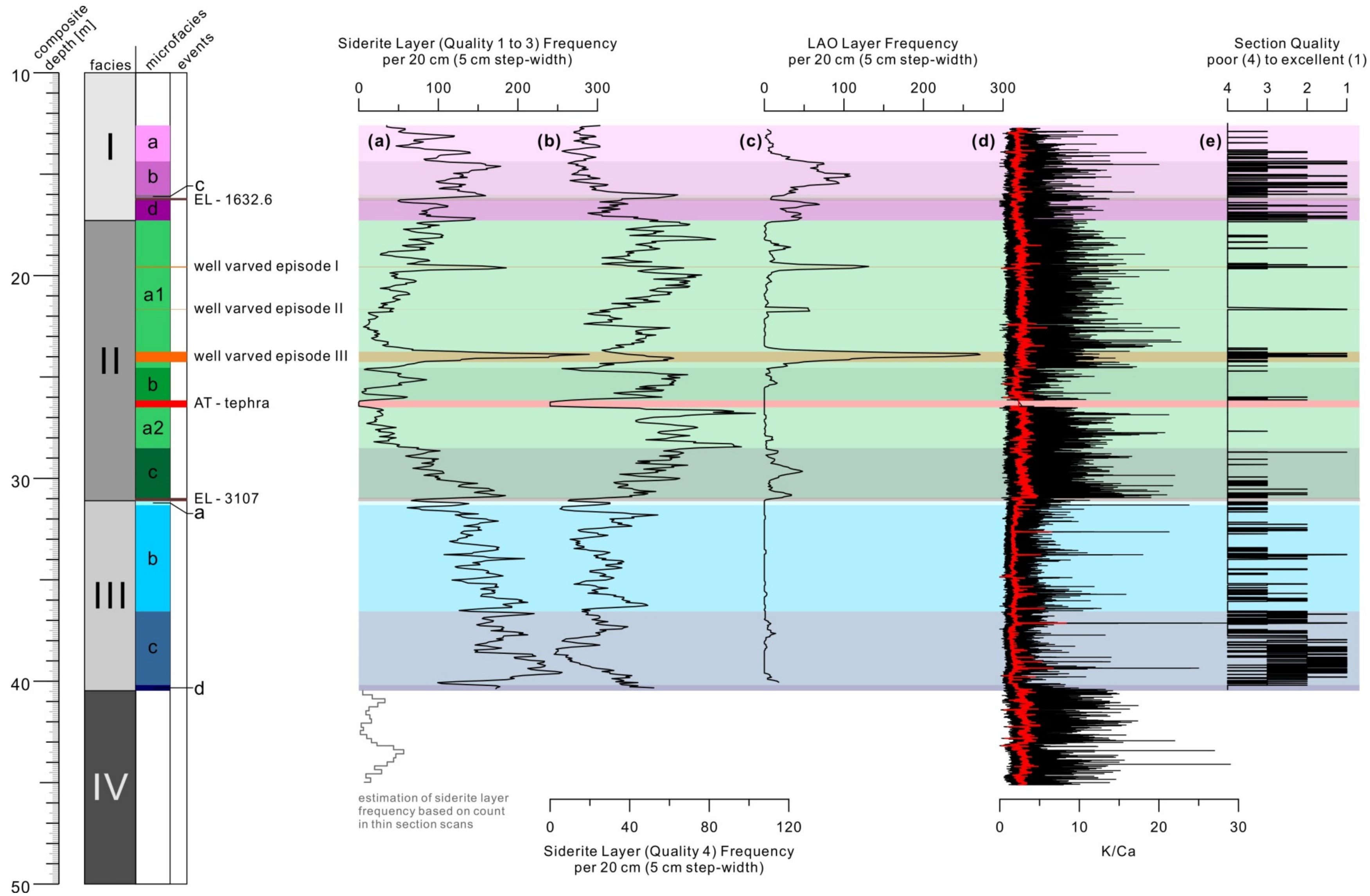
composite depth [m]
facies
microfacies
events
I
II
III
IV
a
b
c
d
a1
a2
EL - 1632.6
well varved episode I
well varved episode II
well varved episode III
AT - tephra
EL - 3107
Siderite Layer (Quality 1 to 3) Frequency per 20 cm (5 cm step-width)
LAO Layer Frequency per 20 cm (5 cm step-width)
Section Quality poor (4) to excellent (1)
(a)
(b)
(c)
(d)
(e)
estimation of siderite layer frequency based on count in thin section scans
Siderite Layer (Quality 4) Frequency per 20 cm (5 cm step-width)
K/Ca

897

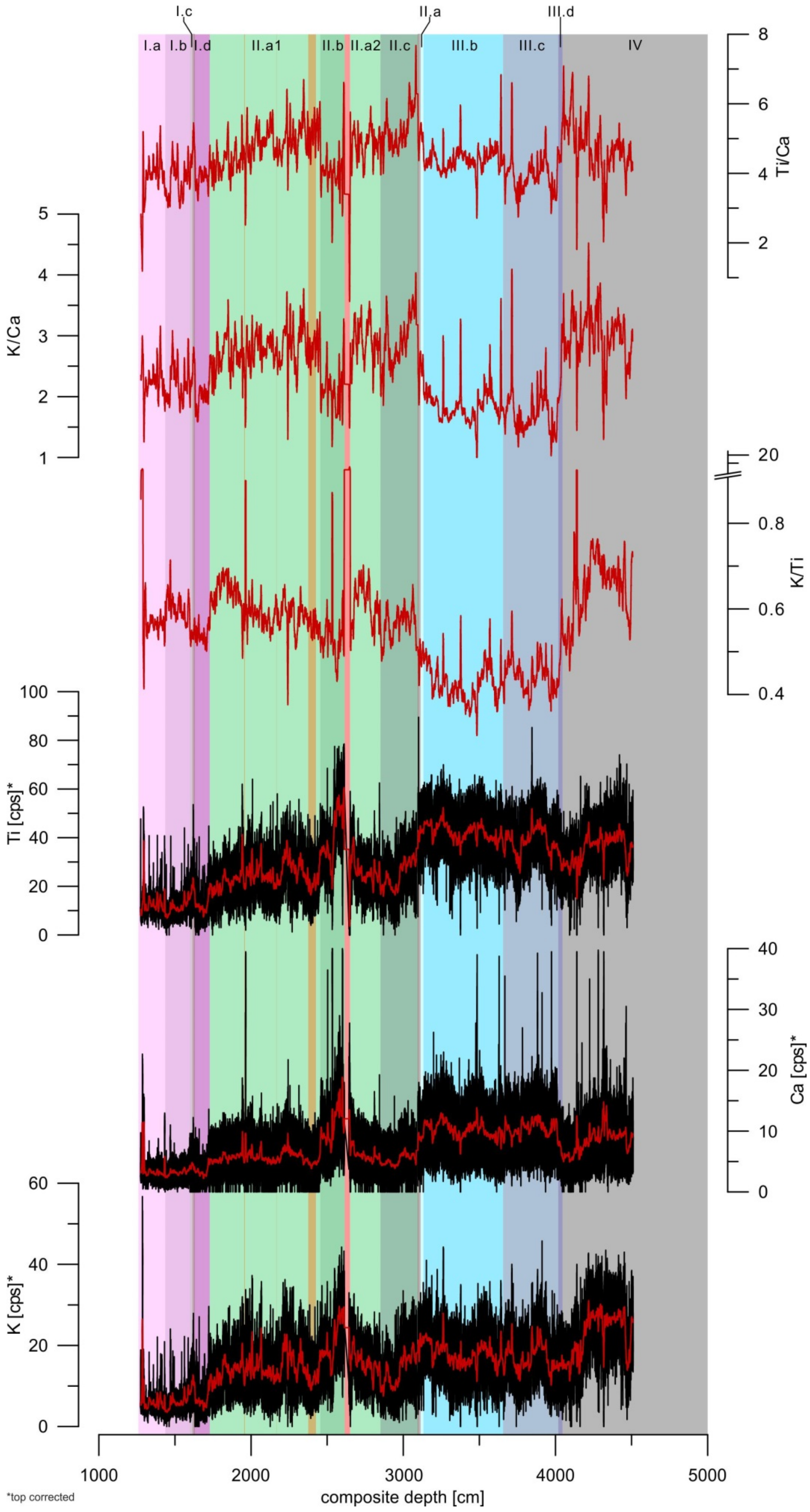

I.c
II.a
III.d
I.a
I.b
I.d
II.a1
II.b
II.a2
II.c
III.b
III.c
IV
Ti/Ca
K/Ca
K/Ti
Ti [cps]*
Ca [cps]*
K [cps]*
composite depth [cm]
*top corrected

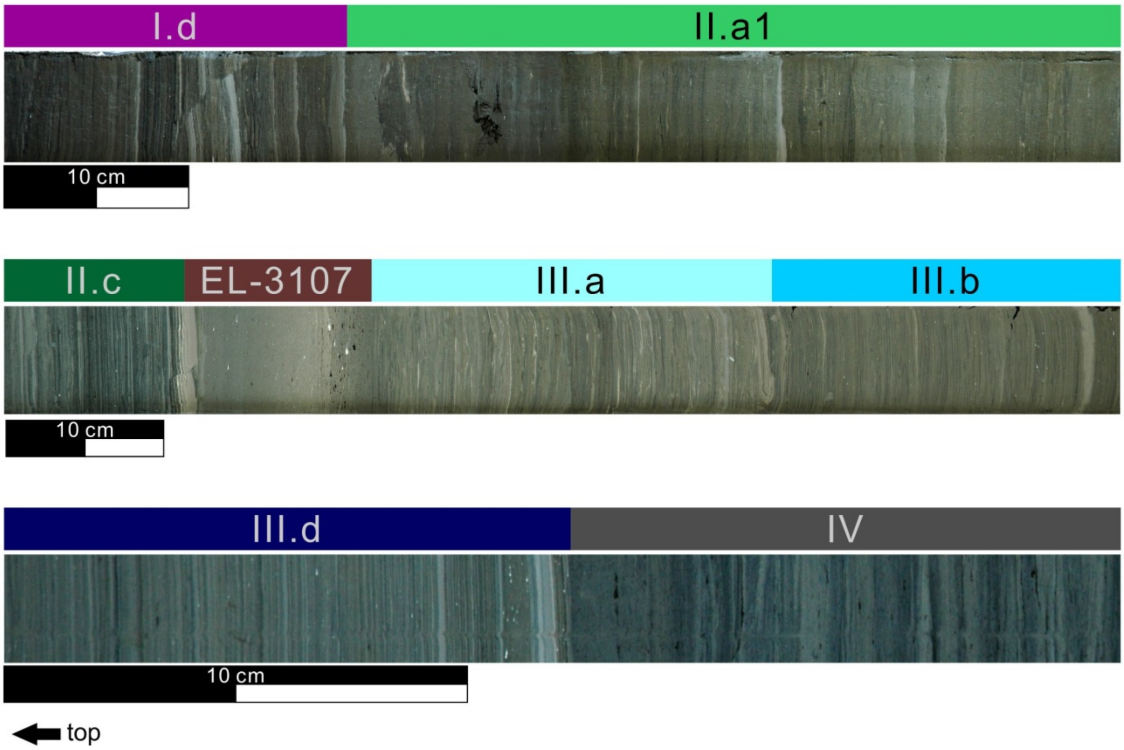

I.d
II.a1
10 cm
II.c
EL-3107
III.a
III.b
10 cm
III.d
IV
10 cm
top

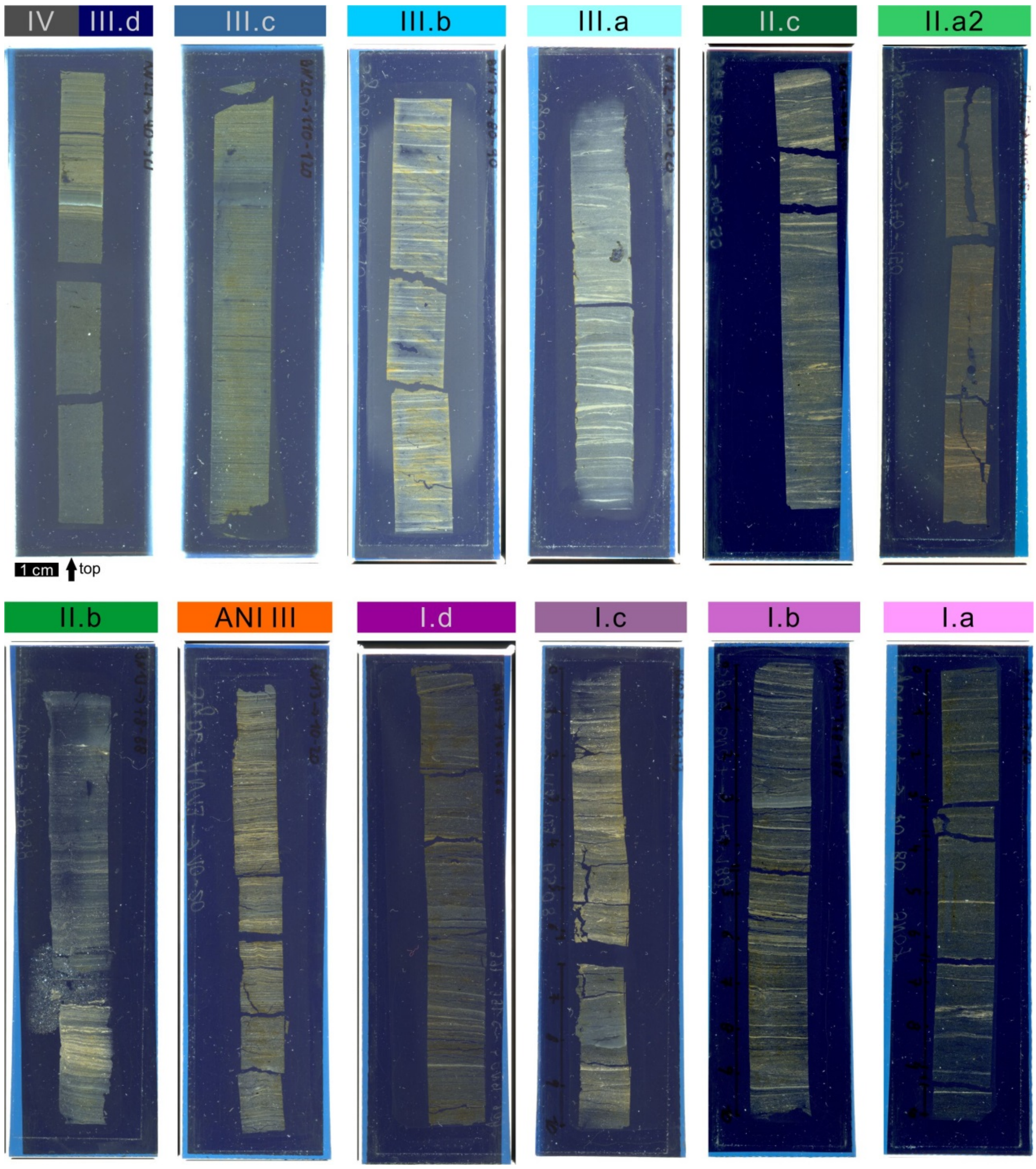
IV
III.d
III.c
III.b
III.a
II.c
II.a2
1 cm
top
II.b
ANI III
I.d
I.c
I.b
I.a

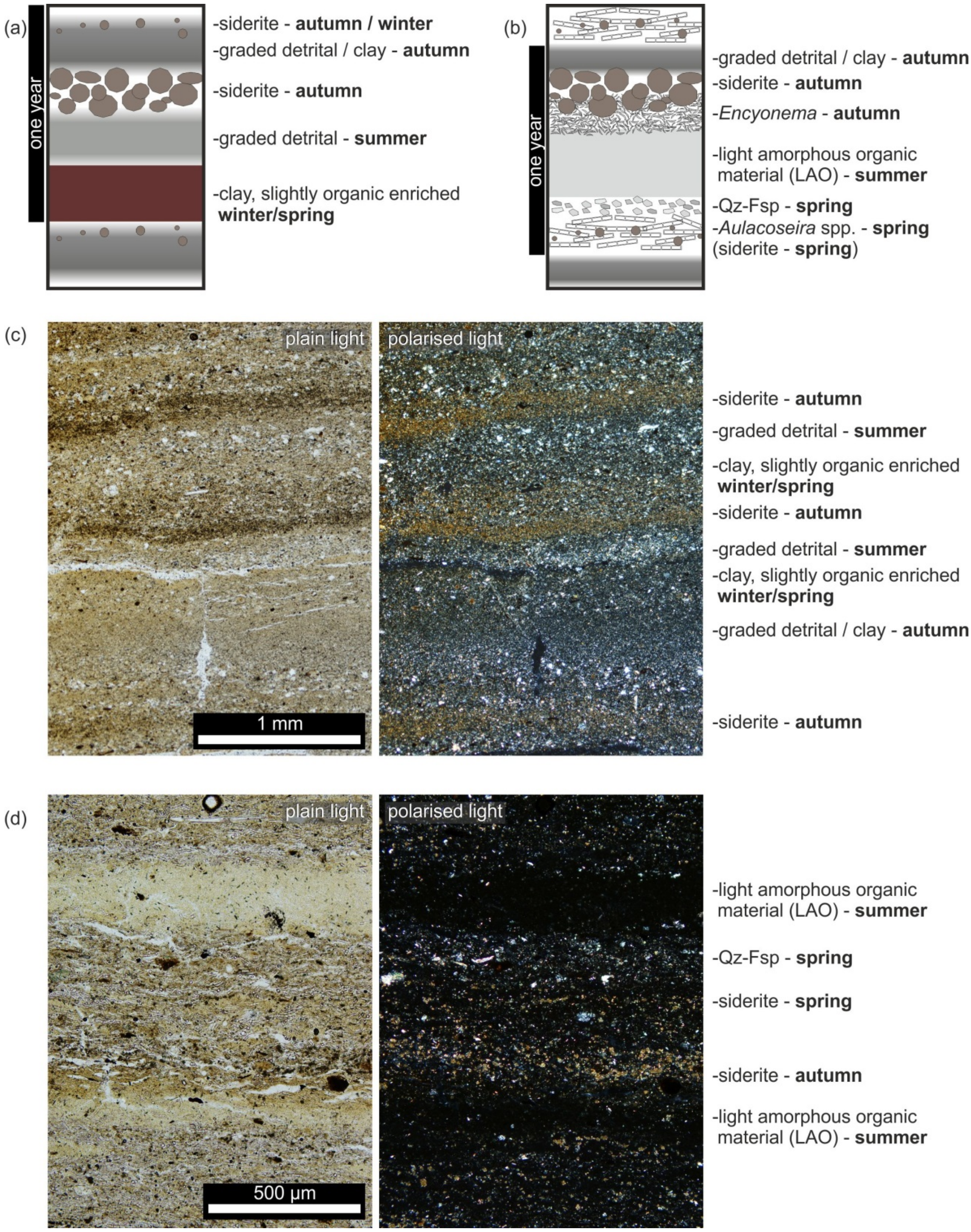
(a)
one year
-siderite - autumn / winter
-graded detrital / clay - autumn
-siderite - autumn
-graded detrital - summer
-clay, slightly organic enriched winter/spring
(b)
one year
-graded detrital / clay - autumn
-siderite - autumn
-Encyonema - autumn
-light amorphous organic material (LAO) - summer
-Qz-Fsp - spring
-Aulacoseira spp. - spring
(siderite - spring)
(c)
plain light
polarised light
1 mm
-siderite - autumn
-graded detrital - summer
-clay, slightly organic enriched winter/spring
-siderite - autumn
-graded detrital - summer
-clay, slightly organic enriched winter/spring
-graded detrital / clay - autumn
-siderite - autumn
(d)
plain light
polarised light
500 µm
-light amorphous organic material (LAO) - summer
-Qz-Fsp - spring
-siderite - spring
-siderite - autumn
-light amorphous organic material (LAO) - summer

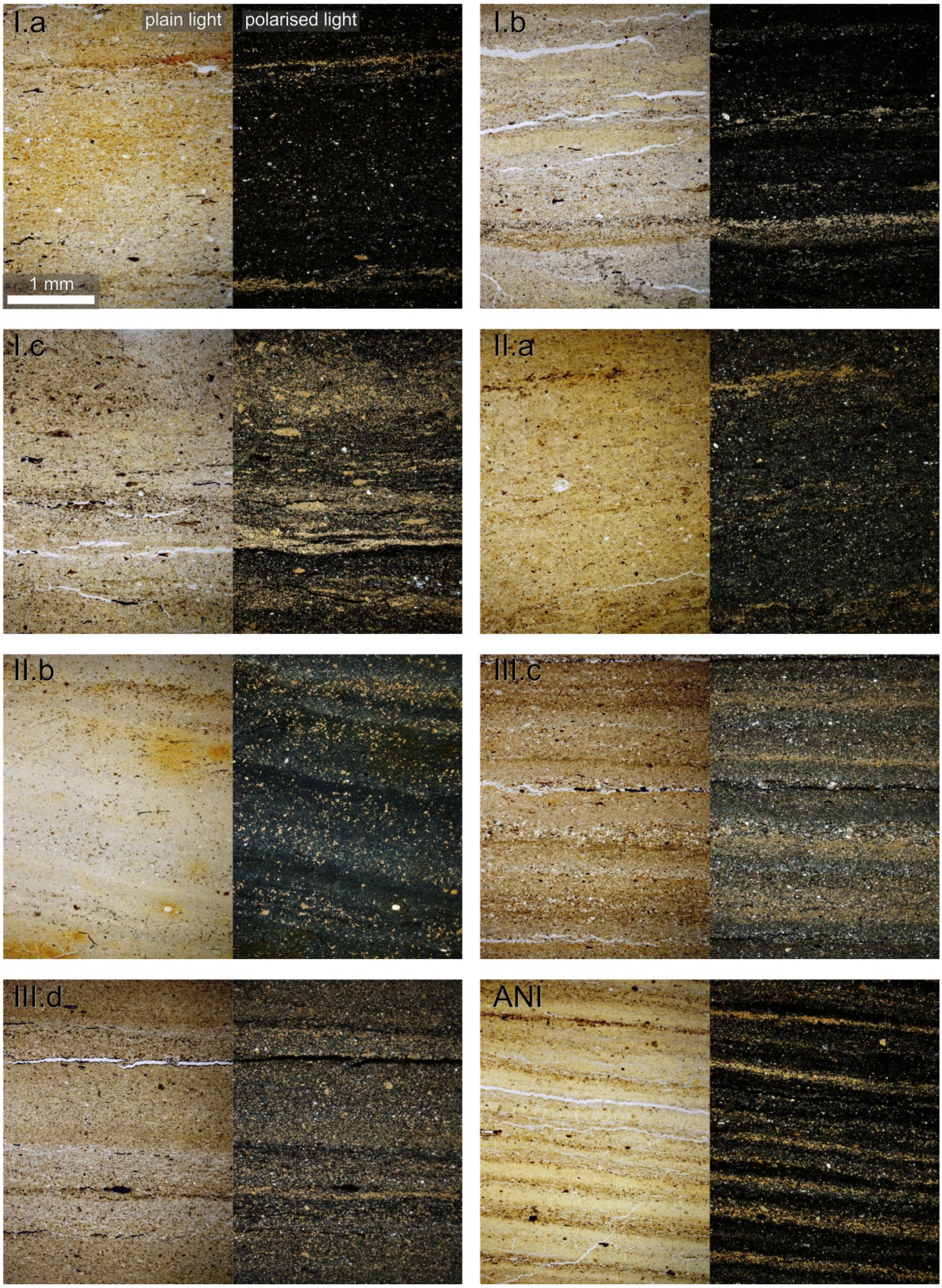

I.a
plain light
polarised light
1 mm
I.b
I.c
II.a
II.b
III.c
III.d
ANI

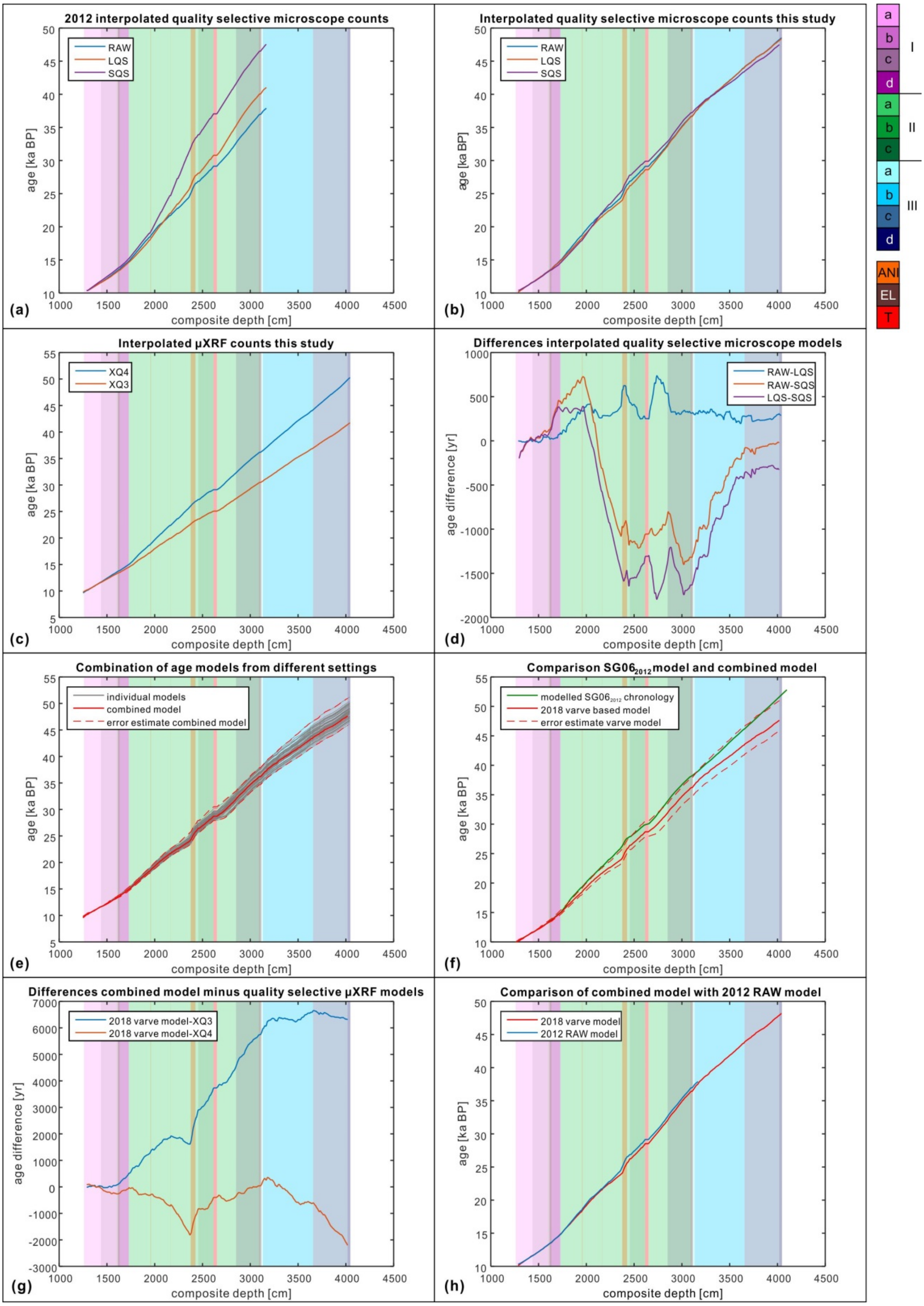

2012 interpolated quality selective microscope counts
RAW
LQS
SQS
age [ka BP]
composite depth [cm]
(a)
Interpolated quality selective microscope counts this study
RAW
LQS
SQS
age [ka BP]
composite depth [cm]
(b)
Interpolated µXRF counts this study
XQ4
XQ3
age [ka BP]
composite depth [cm]
(c)
Differences interpolated quality selective microscope models
RAW-LQS
RAW-SQS
LQS-SQS
age difference [yr]
composite depth [cm]
(d)
Combination of age models from different settings
individual models
combined model
error estimate combined model
age [ka BP]
composite depth [cm]
(e)
Comparison SG06$_{2012}$ model and combined model
modelled SG06$_{2012}$ chronology
2018 varve based model
error estimate varve model
age [ka BP]
composite depth [cm]
(f)
Differences combined model minus quality selective µXRF models
2018 varve model-XQ3
2018 varve model-XQ4
age difference [yr]
composite depth [cm]
(g)
Comparison of combined model with 2012 RAW model
2018 varve model
2012 RAW model
age [ka BP]
composite depth [cm]
(h)
a
b
c
d
I
a
b
c
II
a
b
c
d
III
ANI
EL
T

908 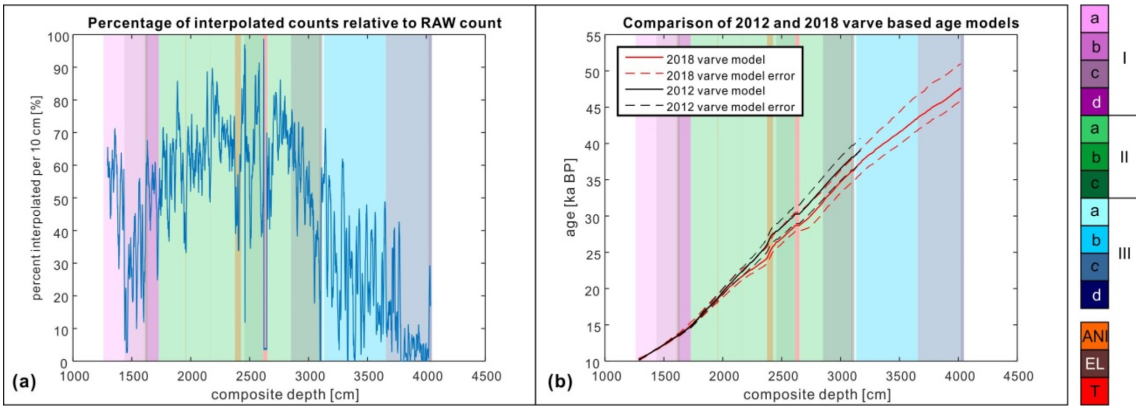

Percentage of interpolated counts relative to RAW count
percent interpolated per 10 cm [%]
composite depth [cm]
(a)
Comparison of 2012 and 2018 varve based age models
2018 varve model
2018 varve model error
2012 varve model
2012 varve model error
age [ka BP]
composite depth [cm]
(b)
a
b
c
d
I
a
b
c
II
a
b
c
d
III
ANI
EL
T